Available online at www.sciencedirect.com
ScienceDirect
Geochimica et Cosmochimica Acta 72 (2008) 5908–5919
Geochimica et Cosmochimica Acta
www.elsevier.com/locate/gca

Kinetic fractionation of Fe isotopes during transport through a porous quartz-sand column

Alan Matthews [a,*], Simon Emmanuel [b], Lena Levi [a], Haim Gvirtzman [a], Yigal Erel [a]

[a] *Institute of Earth Sciences, The Hebrew University of Jerusalem, Edmond Safra Givat Ram Campus, Jerusalem 91904, Israel*
[b] *Department of Geology and Geophysics, Yale University, P.O. Box 208109, New Haven, CT, 06520-8109, USA*

Received 10 March 2008; accepted in revised form 21 September 2008; available online 30 September 2008

Abstract

Sorption and desorption processes are an important part of biological and geochemical metallic isotope cycles. Here, we address the dynamic aspects of metallic isotopic fractionation in a theoretical and experimental study of Fe sorption and desorption during the transport of aqueous Fe(III) through a quartz-sand matrix. Transport equations describing the behavior of sorbing isotopic species in a water saturated homogeneous porous medium are presented; isotopic fractionation of the system ($\Delta_{\text{sorbed metal-soln}}$) being defined in terms of two parameters: (i) an equilibrium fractionation factor, α_e; and (ii) a kinetic sorption factor, α_1. These equations are applied in a numerical model that simulates the sorption-desorption of Fe isotopes during injection of a Fe(III) solution pulse into a quartz matrix at pH 0–2 and explores the effects of the kinetic and equilibrium parameters on the Fe-isotope evolution of porewater. The kinetic transport theory is applied to a series of experiments in which pulses of Na and Fe(III) chloride solutions were injected into a porous sand grain column. Fractionation factors of $\alpha_e = 1.0003 \pm 0.0001$ and $\alpha_1 = 0.9997 \pm 0.0004$ yielded the best fit between the transport model and the Fe concentration and δ^{56}Fe data. The equilibrium fractionation ($\Delta^{56}Fe_{\text{sorbed Fe-soln}}$) of 0.3‰ is comparable with values deduced for adsorption of metallic cations on iron and manganese oxide surfaces and suggests that sandstone aquifers will fractionate metallic isotopes during sorption-desorption reactions. The ability of the equilibrium fractionation factor to describe a natural system, however, depends on the proximity to equilibrium, which is determined by the relative time scales of mass transfer and chemical reaction; low fluid transport rates should produce a system that is less dependent on kinetic effects. The results of this study are applicable to Fe-isotope fractionation in clastic sediments formed in highly acidic conditions; such conditions may have existed on Mars where acidic oxidizing ground and surface waters may have been responsible for clastic sedimentation and metallic element transport.

1. INTRODUCTION

Sorption and desorption processes fundamentally affect the transport properties of metals in a number of important geochemical settings including soil formation and weathering, biogeochemical reactions, and transport in sub-surface geological systems. Stable isotope fractionation may accompany sorption-desorption reactions, and quantitative knowledge of the kinetic and equilibrium fractionation factors is critical if metallic isotopes are to be effectively used to study the cycling of metals in aqueous systems. As sorption-desorption reactions are part of the sedimentary iron isotope cycle, such reactions could influence isotopic fractionation in a wide range of processes, including bacterial and chelating ligand-mediated dissolution of minerals, precipitation of iron Fe(III) minerals from $Fe(II)_{aq}$ solutions in sub-surface groundwater systems, and iron removal from groundwater during water remediation (Brantley et al., 2004; Icopini et al., 2004; Crosby et al., 2005; Johnson et al., 2005; Teutsch et al., 2005; Busigny and Dauphas, 2007; Crosby et al., 2007; Johnson et al., 2008).

* Corresponding author.
E-mail address: alan@vms.huji.ac.il (A. Matthews).

0016-7037/$ - see front matter © 2008 Elsevier Ltd. All rights reserved.
doi:10.1016/j.gca.2008.09.019

Experimental studies on metallic isotope fractionation during sorption–desorption reactions have mostly focused on batch isotope exchange experiments using iron or manganese oxides as the adsorbing solid mineral phase (Johnson et al., 1999; Galy et al., 2002; Rehkämper et al., 2002; Barling and Anbar, 2004; Ellis et al., 2004; Clayton et al., 2005; Pokrovsky et al., 2005, 2008; Malinovsky et al., 2007; Balistrieri et al., 2008; Juillot et al., 2008). Measured isotope fractionation factors (expressed as $\Delta_{\text{sorbed metal-soln}} = \delta_{\text{sorbed ion}} - \delta_{\text{solution ion}}$) vary between 0 and +0.8‰ for metallic ions (e.g., Fe, Cu, Zn), whereas larger negative fractionation factors (0 to –1.8‰) are found for anion species (an extensive summary of fractionation factors may be found in Balistrieri et al., 2008, Table 2). Whilst such experiments provide an excellent insight into elemental and isotopic adsorption fractionation factors in equilibrium systems, they do not shed light on the kinetic fractionation factors for the individual sorption and desorption reactions, the dynamic balance of which controls the overall adsorption. Nor do they address the properties of one of the most potentially powerful adsorbing porous media in natural groundwater flow systems: clastic sandstone aquifers. Fe sorption during paleofluid circulation in the Navajo sandstone aquifer was recognized as a potentially major control of Fe isotope composition by Busigny and Dauphas (2007). Teutsch et al. (2005) examined the Fe-isotopic fractionation in injection experiments conducted at a water remediation site in which Fe(II) in groundwater was adsorbed onto the surfaces of freshly precipitated Fe-oxyhydroxides, and the Fe isotope fractionation was monitored in the extracted pore waters. Using a reactive transport model, Teutsch et al. (2005) found that an equilibrium fractionation factor of $\Delta^{57/54}\text{Fe}_{\text{sorbed Fe-soln Fe(II)}} = 1‰$ best matched their data; Johnson et al. (2008) have alternatively suggested that oxidation of Fe(II) and the formation of ferric oxides/hydroxides was a significant control on Fe isotope composition.

Here, we address the elemental partitioning and metallic isotopic fractionation in a theoretical and experimental study of Fe sorption and desorption during the transport of aqueous Fe(III) through a quartz-sand column. In the theoretical study, we develop transport equations to describe the behavior of sorbing isotopic species in a water saturated homogeneous porous medium, and we present the results of a numerical model that simulates the sorption-desorption of Fe isotopes during injection of an Fe(III) pulse into this medium. In the experimental study we show the results of a series of experiments in which Fe(III) and Na chloride solutions were injected into a porous sand grain column for a finite period at pH 0–2 (the pH range over which aqueous Fe(III) is known to be adsorbed by quartz; Schindler et al., 1976), and then displaced by a tracer-free HCl solution at the same pH. This experimental configuration allows us to both test and apply the kinetic transport theory to the sorption and desorption processes and calculate kinetic isotopic fractionation factors for both these processes as well as the equilibrium adsorption fractionation factor.

2. THEORY

2.1. Transport equations for inert and sorbing metals

The transport of an inert tracer through a homogeneous porous medium can be described by an advection-dispersion equation of the form (Bear, 1972)

$$\frac{\partial C_{\text{M}}}{\partial t} = \nabla \cdot (D_{\text{e}} \nabla C_{\text{M}} - v C_{\text{M}}), \tag{1}$$

where C_{M} is the concentration of the dissolved metal, D_{e} is the dispersion coefficient, and v is the effective transport velocity, often assumed to be equivalent to the interstitial velocity. For sorbing species, however, an additional sink term is required to account for reactions between the surfaces of the solid matrix and the solute. If the solid matrix is comprised of a relatively simple mineral phase, such as quartz, this extra term can be derived by considering the interaction between the sorbate, the surface bonding sites, and the protons in solution, which may also occupy surface sites. In the case of a metal ion, $\text{M}^{\text{n+}}$, this interaction is commonly represented by an equation of the form (Stumm and Morgan, 1996)

$$\text{M}^{\text{n+}} + \text{SH} \underset{\text{k}_{-1}}{\overset{\text{k}_1}{\leftrightarrow}} \text{SM}^{\text{n-1}} + \text{H}^{+}, \tag{2}$$

where SH represents the protonated surface sites, $\text{SM}^{\text{n-1}}$ is the metal-surface complex, and k_1 and k_{-1} are the sorption and desorption rate coefficients, respectively. Clearly, as pH decreases, sorption of the metal becomes less favorable. Two additional reactions also control the protonation of surface sites, represented by

$$\text{H}^{+} + \text{S}^{-} \underset{\text{k}_{-2}}{\overset{\text{k}_2}{\leftrightarrow}} \text{SH}, \tag{3}$$

and

$$\text{H}^{+} + \text{SH} \underset{\text{k}_{-3}}{\overset{\text{k}_3}{\leftrightarrow}} \text{SH}_2^{+}, \tag{4}$$

where k_2 and k_3 are sorption rate coefficients and k_{-2} and k_{-3} are desorption coefficients.

Based on these reactions, a transport equation for the metal ion in a homogeneous porous medium can be written as

$$\frac{\partial C_{\text{M}}}{\partial t} = \nabla \cdot (D_{\text{e}} \nabla C_{\text{M}} - v C_{\text{M}}) + Q_{\text{M}}, \tag{5}$$

where Q_{M} is a net source term representing the net sum of the sorption and desorption reactions; from Eq. (2), this term is defined by

$$Q_{\text{M}} = -\frac{\partial C_{\text{SM}}}{\partial t} = k_{-1} C_{\text{SM}} C_{\text{H}} - k_1 C_{\text{M}} C_{\text{SH}}, \tag{6}$$

with C_{SM} representing the number of bound sites per unit volume of fluid. Typically, the rate of protonation/deprotonation reactions (Eqs. (3) and (4)) is orders of magnitude faster than metal adsorption/desorption (Eq. (2)), and an instantaneous equilibrium condition for these reactions can be assumed (Stumm and Morgan, 1996). Defining the equilibrium constants $K_2 = k_2/k_{-2}$ and $K_3 = k_3/k_{-3}$, the concentrations of C_{SH} and C_{SH2} are given explicitly by

$$C_{SH} = K_2 C_H C_S, \tag{7}$$

and

$$C_{SH_2} = K_2 K_3 C_H^2 C_S. \tag{8}$$

In a uniform porous matrix, the total concentration of occupied and vacant sites is given by the sum $C_S^{tot} = C_S + C_{SM} + C_{SH} + C_{SH2}$, which, if pH is constant, can be used to fully constrain the system. By substituting Eqs. (7) and (8) into the expression for C_S^{tot}, an expression for C_S can be obtained,

$$C_S = \frac{C_S^{tot} - C_{SM}}{1 + K_2 C_H + K_2 K_3 C_H^2}, \tag{9}$$

and a complete model of the system can be constructed using Eqs. (5)–(9). Solutions to the equations for a range of boundary conditions are readily obtained using numerical methods.

2.2. Transport equations for sorbing isotopes

The transport of isotopes with trace abundances is often treated by replacing the concentration term in Eq. (1) with an isotopic ratio (e.g., Blattner and Lassey, 1989). However, for many transition metals (e.g., Fe, Zn and Cu), there may be more than one abundant isotope and it is then necessary to treat the transport of each isotope separately. This caveat was applied to a study of diffusionally controlled Fe-isotope fractionation during diagenetic dolomite concretion formation (Matthews et al., 2004) and subsequently to calculations of equilibrium adsorption fractionation in a reactive transport system (Teutsch et al., 2005).

In this section, we examine a system containing two isotopes, although it can easily be expanded to include any number of isotopic species. In a similar way to the sorption reactions in Section 2.1, we can explicitly represent the behavior of the two isotopes, ^{i}M and ^{j}M, by

$$^{i}M^{n+} + SH \underset{k_{-1}}{\overset{k_1}{\leftrightarrow}} S^{i}M^{n-1} + H^+, \tag{10}$$

and

$$^{j}M^{n+} + SH \underset{\alpha_{-1}k_{-1}}{\overset{\alpha_1 k_1}{\leftrightarrow}} S^{j}M^{n-1} + H^+. \tag{11}$$

Note that in Eq. (11), the sorption and desorption rate coefficients for ^{j}M have been expressed as $\alpha_1 k_1$ and $\alpha_{-1}k_{-1}$, respectively, where α_1 and α_{-1} are uniquely defined kinetic fractionation factors, expected to have values close to unity. Furthermore, when the rate of sorption is equal to the rate of desorption (i.e., at equilibrium) the following two relationships hold:

$$k_1 C_{i_M} C_S = k_{-1} C_{S^iM} C_H, \tag{12}$$

and

$$\alpha_1 k_1 C_{j_M} C_S = \alpha_{-1} k_{-1} C_{S^jM} C_H \tag{13}$$

Dividing Eq. (12) by Eq. (13) and rearranging, we obtain

$$\frac{\alpha_{-1}}{\alpha_1} = \frac{C_{S^iM}/C_{S^jM}}{C_{i_M}/C_{j_M}}, \tag{14}$$

and the ratio α_{-1}/α_1 is therefore equivalent to the conventional definition of the equilibrium fractionation factor, α_e, defined as

$$\alpha_e = \left(\frac{(^{i}M/^{j}M)_{sorbed}}{(^{i}M/^{j}M)_{solution}} \right)_e, \tag{15}$$

where $(^{i}M/^{j}M)_{sorbed}$ is the isotopic ratio of the sorbed metal, $(^{i}M/^{j}M)_{solution}$ is the isotopic ratio of the metal in solution, and the subscript e indicates equilibrium. Thus, $\alpha_{-1} = \alpha_e \alpha_1$ and the isotopic fractionation of a non-equilibrium system can be described in terms of two parameters: (i) an equilibrium fractionation factor, α_e; and (ii) a kinetic factor, α_1. Clearly, if a system is near or at equilibrium, isotopic fractionation between the sorbed and dissolved metal is determined only by α_e; such conditions are achieved when the rate of mass transfer is low relative to the rate of reaction. Criteria for recognizing near-equilibrium states are discussed in Section 2.3.

To describe the transient transport of the isotopes and the evolution of the isotopic ratios in the system requires separate transport equations for each isotope:

$$\frac{\partial C_{i_M}}{\partial t} = \nabla \cdot (D_e \nabla C_{i_M} - v C_{i_M}) + Q_{i_M}, \tag{16}$$

and

$$\frac{\partial C_{j_M}}{\partial t} = \nabla \cdot (D_e \nabla C_{j_M} - v C_{j_M}) + Q_{j_M}. \tag{17}$$

Similar to Eq. (6), the two sink terms are given by

$$Q_{i_M} = -\frac{\partial C_{S^iM}}{\partial t} = k_{-1} C_{S^iM} C_H - k_1 C_{i_M} C_{SH}, \tag{18}$$

and

$$Q_{j_M} = -\frac{\partial C_{S^jM}}{\partial t} = k_{-1} C_{S^jM} C_H - k_1 C_{j_M} C_{SH}, \tag{19}$$

As in Section 2.1, C_{SH} and C_{SH2} are given by Eqs. (7) and (8), and if pH is constant and uniform throughout the system, the series of equations is closed by the definition of the total site concentration ($C_S^{tot} = C_S + C_{iSM} + C_{jSM} + C_{SH} + C_{SH2}$), which can be rearranged to obtain an expression for C_S,

$$C_S = \frac{C_S^{tot} - C_{S^iM} - C_{S^jM}}{1 + K_2 C_H + K_2 K_3 C_H^2}. \tag{20}$$

Thus, the isotopic evolution of a system is determined by transport parameters (v and D_e), the concentration of surface sites (C_S^{tot}), rate coefficients (k_1, k_{-1}), equilibrium constants (K_2, K_3), and fractionation factors (α_e,α_1), and numerical solutions to Eqs. (7), (8) and (16)–(20) can be obtained for different boundary conditions. As discussed in Section 2.3, if a sufficiently wide range of experimental conditions are examined, all of these parameters, including the kinetic fractionation factors, can be experimentally determined.

The model presented here differs from most previous models dealing with the transport and sorption of iron isotopes (e.g., Matthews et al., 2004; Teutsch et al., 2005) for three main reasons: (1) the interaction of the metal species with the solid matrix is considered to be a dynamic, rather

than an equilibrium, process; (2) both sorption and desorption reactions are explicitly modeled; (3) the effect of pH on the availability of surface sites is explicitly included. Furthermore, such a model should be capable of describing the transport of Fe through a sand column; ^{56}Fe and ^{54}Fe typically represent ~92% and ~6%, respectively, and treating the transport of the two isotopes separately is necessary to successfully model the evolution of isotopic signatures which result from the combination of transport and sorption–desorption processes.

2.3. Numerical modeling and model behavior

The models described in Sections 2.1 and 2.2 are relatively complex, and the influence of each of the parameters on the evolution of metal concentrations and isotopic patterns is not immediately apparent. Here, we use a brief parametric analysis to show the impact of the various model inputs on concentration and isotopic breakthrough curves and to demonstrate the numerical stability of the solutions.

To simulate the sorption–desorption properties of Fe isotopes when a pulse of Fe(III) solution is injected into a quartz matrix, the coupled equations determining the transport of metal species and their isotopes outlined in Sections 2.1 and 2.2 are solved here numerically using a finite element method utilizing the Multiphysics® software package (COMSOL). One code was constructed to solve the set of equations in Section 2.1, while a second, separate code solved the system of equations for isotopic transport outlined in Section 2.2. To mimic the flow of a metal through a homogeneous porous column, a 1D domain was constructed from a mesh of 960 Lagrange quadratic elements. The numerical solutions were found to be stable for a wide range of parameters, and both the time dependent linear system solver and the solutions were shown to be insensitive to increased grid density. Analysis of the calculations also demonstrated that mass was conserved in the simulations.

Simulation of a pulse input for a single metal species (C_M) into a porous media saturated with interstitial metal-free solution, followed by its displacement by metal-free solution, was achieved by applying a constant concentration at the inlet for a limited duration; a standard Neumann boundary condition ($\partial C_M/\partial x = 0$) was set at the outlet, corresponding to a purely advective solute output. The simulations were conducted at pH values 0, 1, and 2, respectively (i.e., at each pH value, the simulations were performed with the same pH values for the metal-bearing and metal-free solutions). The evolution of ^{56}Fe at the outlet in the isotope model was simulated by applying similar boundary conditions, with the concentrations of ^{54}Fe and ^{56}Fe at the inlet being determined from the total metal concentration and the reported values of the Fe IRMM-14 standard (5.845% and 91.754%, respectively). The δ^{56}Fe value of the input solution was arbitrarily set at 0‰. Values for K_2 ($10^{1.6}$ μM^{-1}) and K_3 ($10^{-7.6}$ μM^{-1}) were adopted from the protonation constants for quartz proposed by Sverjensky and Sahai (1996) for the diffuse double layer model. In the model, the fractionation factors were defined as

$$\alpha_e = \left(\frac{(^{56}Fe/^{54}Fe)_{sorbed}}{(^{56}Fe/^{54}Fe)_{solution}}\right)_e, \quad (21)$$

and $k_1^{54} = \alpha_1 k_1^{56}$. (Note that equilibrium fractionation factors expressed using the Δ notation are related to α_e by the relation: $\Delta_{\text{sorbed metal-soln}} = \delta_{\text{sorbed ion}} - \delta_{\text{solution ion}} \approx 1000 \ln\alpha_e$).

The influence of each of the key model parameters on the solute breakthrough curve is shown in Fig. 1. In most of the simulations presented here three stages can be observed: (1) Fe concentrations slowly increase at the outlet, reflecting the adsorption of Fe onto the quartz matrix; (2) plateau in Fe concentration, indicating that surface sites are approaching saturation with respect to Fe and a state of chemical equilibrium; and (3) Fe concentrations decrease as desorption dominates. Overall, system behavior is very consistent and a number of generalizations can be made:

- The asymmetry of the adsorption and desorption phases is an indicator of the proximity of the system to chemical equilibrium. For example, in Fig. 1a the simulation at pH 0 indicates that near-instantaneous equilibrium is maintained throughout, whereas at pH 1 the long tail apparent in the desorption phase indicates that disequilibrium is present.
- As pH increases and more surface sites become available for binding Fe, the degree of retardation—measured by the rate at which concentrations increase at the inlet—increases significantly (Fig. 1a).
- Increasing the value of k_1 directly increases the rate of sorption, resulting in a decreased mean rate of transport through the system (Fig. 1b).
- By contrast, raising the value of k_{-1} acts to increase the rate of mass transfer by promoting the desorption of metal ions from the surface (Fig. 1c),
- Increasing the concentration of surface sites promotes sorption, effectively retarding solute transport (Fig. 1d). Note that increasing retardation also leads to increased tailing at long times, reflecting the shift away from Fickian transport due to the influence of surface reactions.

The influence of α_1 and α_e on the value of δ^{56}Fe recorded at the outlet is shown in Fig. 2, and the three stages (sorption, steady state, and desorption) can also be observed in the evolving isotopic compositions. During the initial sorption stage, δ^{56}Fe values decrease to a minimum value of around −1 ‰ and then gradually increase, in some cases slightly exceeding 0‰; however, as the surface sites become saturated with Fe, the isotopic signature approaches a plateau with a value close to 0‰ in all cases. During the desorption stage, all simulations show an initially positive δ^{56}Fe value reflecting a release of the heavy isotope that had preferentially accumulated on the surface of the quartz; at later times, however, values can become increasingly positive or increasingly negative.

Despite the relative complexity of the model, some generalizations can be made concerning the effect of α_1 and α_e on the evolution of δ^{56}Fe. As α_1 decreases the isotopic trough marking the initial breakthrough becomes increas-

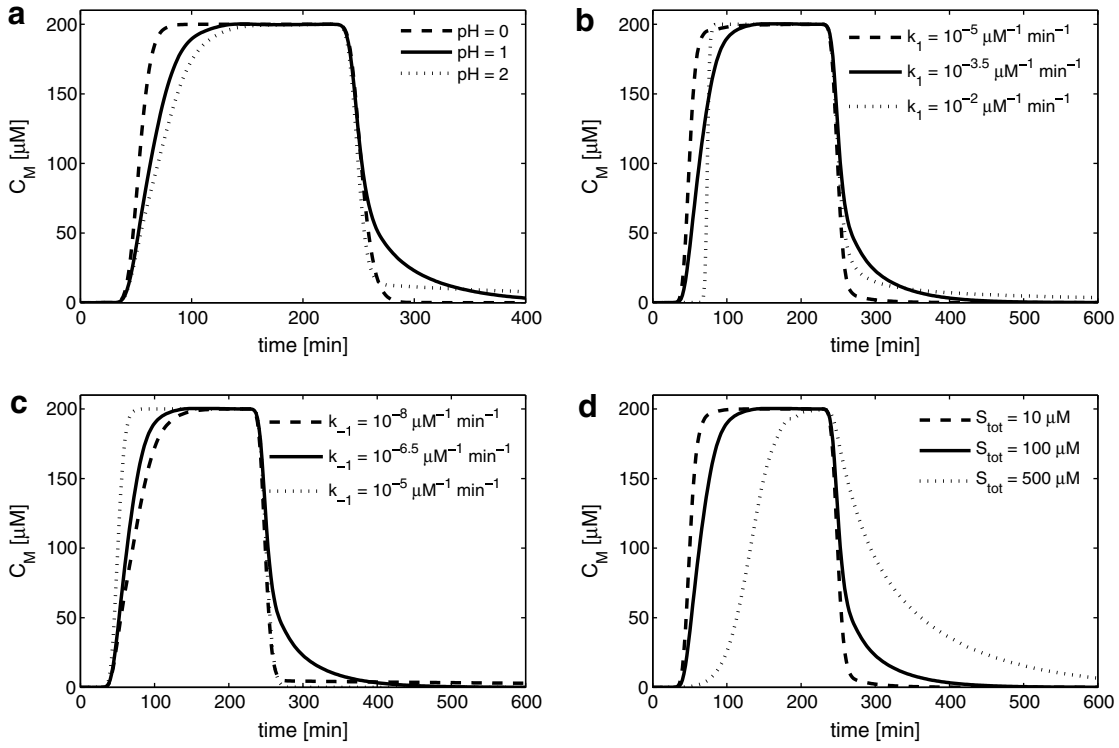

Fig. 1. Effect of different model parameters on the breakthrough curve of a sorbing metal species. (a) pH; (b) k_1; (c) k_{-1}; and (d) C_S^{tot}. Unless otherwise indicated, parameter values are $v = 1$ cm min^{-1}, $D_e = 0.5$ cm^2 min^{-1}, $k_1 = 10^{-3.5}$ μM^{-1} min^{-1}, $k_{-1} = 10^{-6.5}$ μM^{-1} min^{-1}, $K_2 = 10^{1.6}$ μM^{-1}, $K_3 = 10^{-7.6}$ μM^{-1}, $C_s^{tot} = 100$ μM, and pH 1. The input pulse has a concentration of 200 μM and duration 200 min. Column length is 50 cm.

ingly negative i.e., $\Delta_{\text{sorbed metal-soln}}$ becomes more negative (Fig. 2a). This occurs because decreasing values of α_1 lead to lower values for k_1^{54} and a correspondingly lower rate for ^{54}Fe adsorption. Thus, the sorbed phase becomes increasingly enriched in ^{56}Fe while the dissolved Fe becomes increasingly depleted. By contrast, for the set of parameters explored in the simulations, the equilibrium fractionation factor, α_e, has little effect on the magnitude of the initial trough. The equilibrium fractionation factor does, however, determine whether or not δ^{56}Fe is positive or negative as the system approaches the equilibrium plateau stage (Fig. 2b), with higher values of α_e producing more negative values of δ^{56}Fe; for a fixed value of α_1, higher values of α_e also correspond to increasing values of α_{-1} (Eq. (14)), which in turn result in higher rates of ^{54}Fe desorption relative to ^{56}Fe and a depletion of ^{56}Fe in the solution.

The rate coefficients, k_1 and k_{-1}, also have a strong impact on the isotopic composition recorded in the outlet solution (Fig. 2c–d). Higher values of k_1 serve to amplify the degree of isotopic fractionation recorded during the initial breakthrough stage, while higher values of k_{-1} reduce the initial fractionation effect; such behavior reflects the relative dominance of the sorption and desorption processes and their respective effects on fractionation.

Even when $\alpha_e = 1$, the transient isotopic signatures may still reflect kinetic fractionation (Fig. 2b). Ultimately, however, whether or not the equilibrium fractionation factor is sufficient to describe the system is dependent on the proximity of the system to equilibrium, which is determined by the relative time scales of mass transfer and chemical reaction. Thus, low fluid transport rates should produce a system that is less dependent on kinetic effects. In experimental systems, however, the degree of disequilibrium can be estimated from the level of asymmetry of the concentration breakthrough curve.

3. EXPERIMENTAL DESIGN AND METHODS

The pulse-displacement experiments were conducted in a cylindrical homogeneously packed sand column, 5 cm in diameter and 50 cm in length. This porous media was always saturated with interstitial fluid and a laminar flow regime was maintained in all experiments so that Darcy's law is valid. Input Fe(III) solutions were made by dissolving $FeCl_3$ in HCl solutions at pH values of 0, 1 and 2. Two Fe solution concentrations were used: 208 μM (*ca* 10 ppm) and ~1900 μM (*ca* 100 ppm, respectively). In a single experiment at pH of 0, 500 μM Na solutions were used as a conservative inert tracer. Prior to the input of the Fe(III) or Na solutions, the compacted sand column was saturated with HCl solution at the pH of the experiment: the displacement of the metal pulse was similarly made with HCl solution at the same pH, thus ensuring that both pH and chloride concentrations were uniform throughout. The sand comprised natural pure quartz (>99%) with a mean grain size ~500 μm and inclusive standard deviation 0.39 phi, classifying it as well-sorted. The measured porosity was 0.347 and the surface area calculated from this

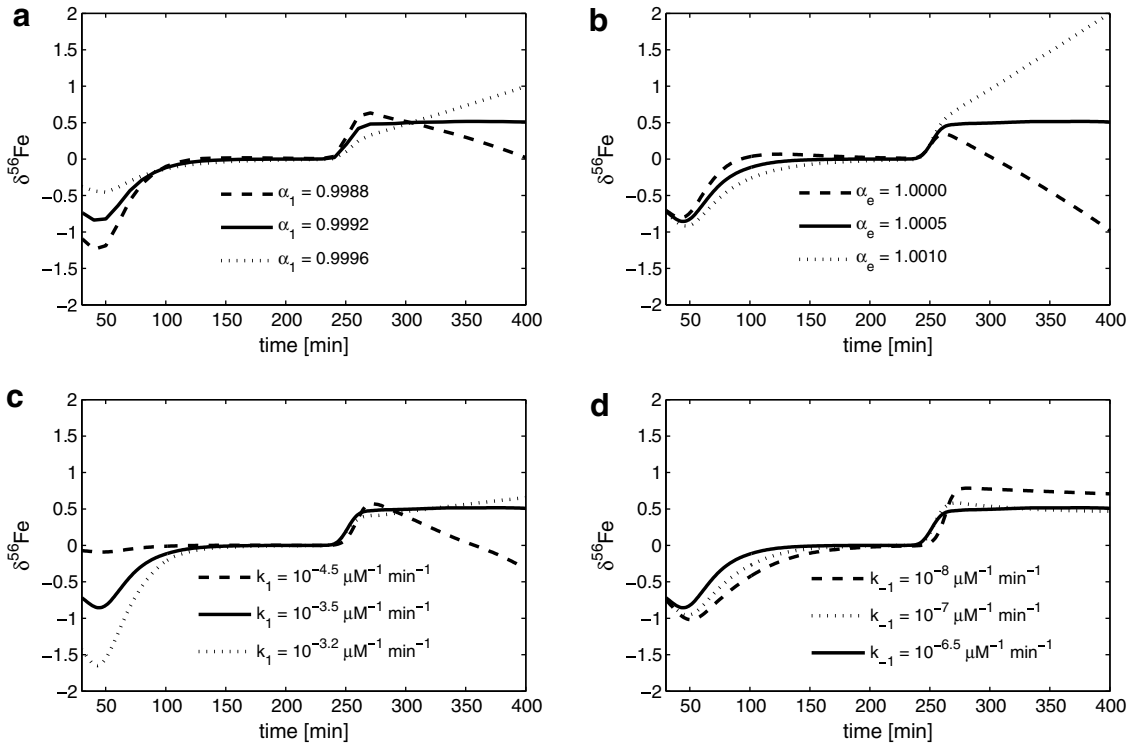

Fig. 2. Effect of fractionation factors and rate constants on isotopic evolution in the outlet solution. Results are shown for (a) α_1; (b) α_e; (c) k_1; and (d) k_{-1}. Unless otherwise indicated, parameter values are $\alpha_e = 1.0005$, $\alpha_1 = 0.9992$, $k_1 = 10^{-3.5}$ μM^{-1} min^{-1}, $k_{-1} = 10^{-6.5}$ μM^{-1} min^{-1}, $v = 1$ cm min^{-1}, $D_e = 0.5$ cm^2 min^{-1}, $K_2 = 10^{1.6}$ μM^{-1}, $K_3 = 10^{-7.6}$ μM^{-1}, $C_s^{tot} = 100$ μM, and pH 1. The input pulse has an isotopic signature of $\delta^{56}Fe = 0‰$ and a concentration of 200 μM. Duration of the pulse is 200 min and column length is 50 cm. The total concentration breakthrough curve at pH 1 is depicted in Fig. 1a; note that although large fractionations occur at early and long times, corresponding concentrations are low (Fig. 1). To give a clearer picture of the important stages of the breakthrough curve, the x axis begins at $t = 30$ min.

porosity and the grain-size distribution, assuming spherical geometry for the quartz grains was 5.47 m^2. Full details of the sand preparation, grain size distribution and porosity measurements are given in Levi (2005).

The experimental apparatus is illustrated in Fig. 3. The cylindrically packed vertical sand column is connected to two feed lines with a T-connection fitting, allowing the selection of the influent line. Two large volume glass (Marriott) bottles are connected to the pump, one for the metal-free HCl solution at the pH of the experiment (i.e., HCl solutions made up with deionized water at the desired pH), the second for the $FeCl_3$ or NaCl solutions in HCl at the desired pH. The entrance of each bottle is sealed with a plastic cork to ensure that air entrance only occurs through a plastic tube inserted through the cork. Thus, at point A the bottle is open to the air (i.e., the pressure is equal to the atmospheric pressure) and at any point above A and below the water surface, the pressure is less than atmospheric.

The simultaneous use of two large volume bottles decreases fluctuations in flow by providing a constant water-head upstream of the pump. The metal-free and metal-bearing solutions are pumped at similar flow rates using a peristaltic pump (Cole-Parmer Console Drive) through silicone tubing inserted into the plastic tubes in the bottles at one end, and to the entrance of the column at the other end. The influent solution can be switched at the required time (e.g., on cessation of the tracer pulse) using the T-connections at the entrance. While solution from one bottle enters the column, the solution from the second bottle flows through the bypass line to discharge and vice versa. Samples were collected at the outlet of the column and samples representing the input solutions were collected from the bypass lines located 2 cm before the entrance. Na and Fe concentration measurements were made with a Perkin Elmer 5100 Atomic Adsorption Spectrometer. All samples were acidified to pH 1 prior to analysis. Measurements of pH were carried out using a WTW 196 pH meter.

Fe isotope analyses were made by MC-ICP-MS, as described by Belshaw et al. (2000), Zhu et al. (2002) and Matthews et al. (2004). Since the solutions were prepared from pure reagents free of matrix contaminants, chromatographic purification was not used prior to the isotopic analysis. The experimental solutions were first evaporated to dryness then brought to either 10 or 5 ppm Fe concentration using 0.1 M HCl, before being introduced to the plasma through a desolvating nebuliser without N_2 gas flow to eliminate interferences associated with ArN and hydroxide species. All isotopic measurements (most in replicate) were made as $^{57}Fe/^{54}Fe$ ratios using sample-standard bracketing against the IRMM-14 metal standard. This particular isotope ratio is measured because the collector assembly of the Nu Instruments MC-ICP-MS used for this work (Geological Survey of Israel) is configured for the measurement

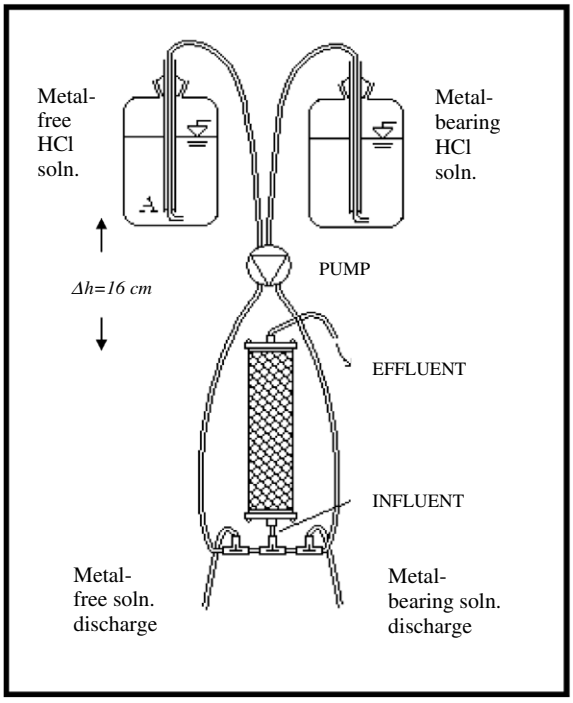

Fig. 3. Experimental apparatus. The diagram illustrates the scheme for the sequential introduction of the metal-bearing and metal-free HCl solutions from two glass Marriott bottles (shown at top).

of $^{57}Fe/^{54}Fe$ and $^{57}Fe/^{56}Fe$ ratios, but not $^{56}Fe/^{54}Fe$ ratios. In order to convert the analytical data to $\delta^{56}Fe$ values used in the model calculations, the measured $\delta^{57}Fe$ values were transformed using the mass-dependent relationship: $\delta^{56}Fe = 0.68 * \delta^{57}Fe$. Independent measurements of $^{57}Fe/^{54}Fe$ and $^{57}Fe/^{56}Fe$ ratios for a wide range of natural and artificial solutions show that measured isotope ratios follow the mass fractionation relation. The $\delta^{57}Fe$ value (relative to IRMM-14) of the input solution is -0.13 ± 0.06 ‰, giving a $\delta^{56}Fe$ value of -0.08 ‰.

Experimental conditions are given in Table 1. In total six experiments were performed: the first experiment (experiment #1) employed Na as a tracer (502 μM; pH 1), three experiments used 208 μM Fe solutions at pH 0, 1 and 2 (experiments #2, #3, #4, respectively), while two additional experiments were conducted with 1900 μM Fe at pH 1 and 2 (experiments #5 and #6, respectively). Each experiment consisted of a step input phase during which the Fe or Na solution was injected into the sand column containing HCl solution at the experimental pH. When the output solution concentration equaled the input solution concentration (the plateau phase), the configuration was reversed, thereby terminating the step input and allowing the interstitial Fe solution to be displaced by pure HCl solution at the experimental pH. Fe isotope measurements were made for the 208 and 1900 μM experiments at pH 1 and for the 208 μM experiment at pH 2. All experimental results are detailed in Electronic Annex EA-1.

4. EXPERIMENTAL RESULTS AND DISCUSSION

The experimental data were used to optimize the model parameters using a sequential approach. The dispersion coefficient, D_e, was first obtained by employing an error minimization technique that compared solutions to the advection-dispersion equation (Eq. (1)) with the Na breakthrough data. Specifically, an objective function, defined as the sum of the errors between the measured and predicted values, was minimized using a MATLAB algorithm based on the Nelder-Mead method. Once D_e was obtained, a similar technique was applied to the Fe concentration data to isolate k_1 and k_{-1}; values for the protonation constants K_2 and K_3 were estimated from calculated literature values for quartz (Sverjensky and Sahai, 1996). Finally, using the previously obtained parameters, the fractionation factors, α_e and $\alpha_{1,}$ were extracted by applying the error minimization method to the Fe isotope data. In the second and third sequential phases, data from pH 2 experiments were disregarded owing to irreversible iron oxide precipitation; this point will be discussed in detail later in this section.

The concentration breakthrough curves for the different experiments are shown in Fig. 4 and a summary of the model parameters produced by fitting the numerical model to the experimental results is shown in Table 2. Importantly, it can be seen that for the inert Na tracer, Eq. (1) produces an excellent fit with the experimental data (Fig. 4a), confirming that the advection-dispersion equation adequately represents the transport of solute through the column. Anomalous (non-Fickian) transport is often observed during mass transfer in porous media (Domenico and Schwartz, 1997; Fetter, 1988), and the symmetrical Fickian behavior found here is probably due to the homogeneous packing of the column. Although the dispersion coefficient is usually considered to be a function of fluid velocity (Bear, 1972), the range of flow rates in the Fe experiments differed from the Na tracer experiments by less than 25% and a value of 0.5 $cm^2\ min^{-1}$ is therefore assumed in the sorption and isotopic transport models as well.

Table 1
Conditions for the different experiments

Experiment No.	1	2	3	4	5	6
Solute species	Na	Fe	Fe	Fe	Fe	Fe
Input concentration [μM]	502	208	208	208	1934	1898
pH	1	0	1	2	1	2
Pulse duration, t_1 [min]	161.9	202.2	161.7	262.2	206.4	304.5
Interstitial velocity, $t < t_1$ [cm min^{-1}]	0.96	0.97	0.96	0.93	1.00	0.99
Interstitial velocity, $t > t_1$ [cm min^{-1}]	0.94	0.92	0.74	0.90	0.85	0.82

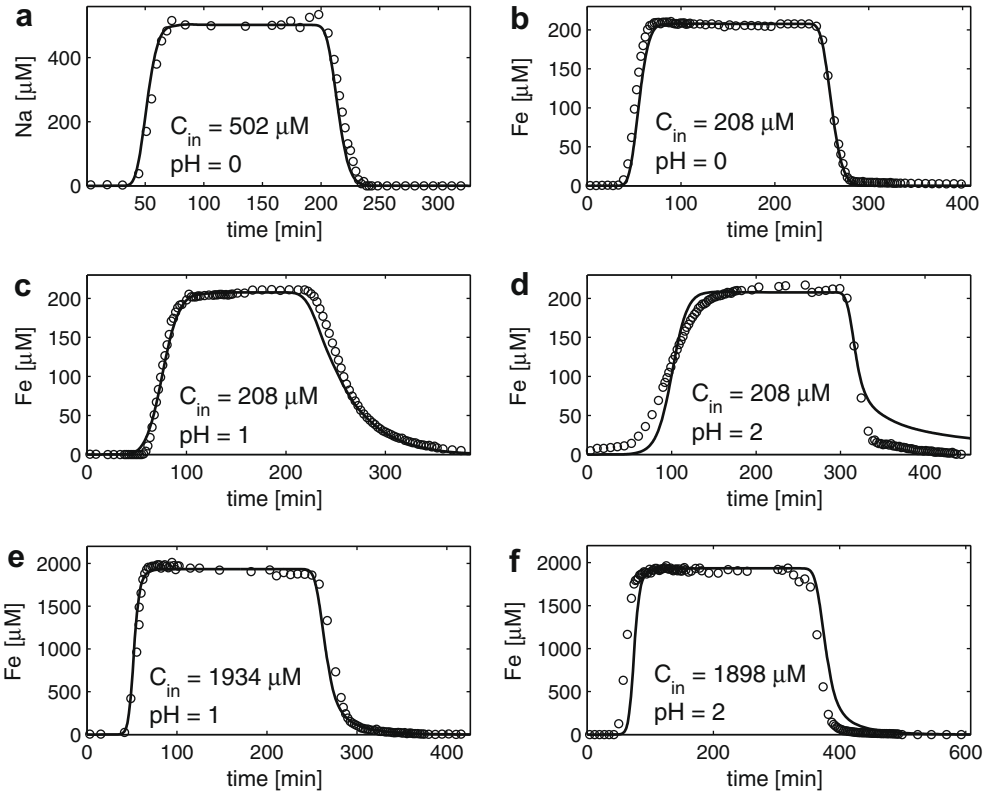

Fig. 4. Experimental breakthrough data for (a) Na and (b–f) Fe solutions. Inlet concentrations (C_{in}) and pH are indicated for each experiment. Summary of experimental conditions is given in Table 1. Solid lines indicate the model breakthrough curves.

Table 2
Summary of model parameters

Fitted parameters	Value	Units
D_e	0.5	$cm^2\ min^{-1}$
k_1	$6.31 * 10^{-4}$	$\mu M^{-1}\ min^{-1}$
k_{-1}	$1.26 * 10^{-6}$	$\mu M^{-1}\ min^{-1}$
[a]K_2	$3.98 * 10^{1}$	μM^{-1}
[a]K_3	$2.51 * 10^{-8}$	μM^{-1}
C_S^{tot}	$2.00 * 10^{2}$	μM
α_1	0.9997	
α_e	1.0003	

[a] Sverjensky and Sahai (1996).

The flow through experiments involving Fe show asymmetric breakthrough curves typical of sorption/desorption behavior and there was a good agreement between the Fe concentration data and the model discussed in Section 2.3. For Fe concentrations of ~200 μM (Fig. 4b–d), the sorption model (Eqs. (5)–(9)) successfully reproduces the solute breakthrough curves for the pH range 0–2. However, it is important to note that at pH 2 the model significantly overestimates the concentration of Fe during desorption phase (Fig. 4d). This effect could be due to a small degree of irreversible Fe-adsorption or precipitation of Fe-oxyhydroxides on the surface of the quartz matrix, a process that is not accounted for in the sorption model. Clearly, when the sorption reactions are completely reversible, all the input solute pulse would be removed from the system as complete desorption occurs. However, if a portion of the solute mass is irreversibly fixed within the porous matrix, this portion will not be transferred back to the solution phase and the model will overestimate the Fe concentration during desorption. At higher Fe concentrations (~2000 μM), however, no such tailing effects are observed and the agreement between model and experiment is very good (Fig. 4e–f), due to the rapid saturation of surface sites, relatively little retardation occurs, even at pH 2.

The value obtained for the density of total surface sites C_S^{tot} (200 μM) is consistent with estimates reported elsewhere (Schindler and Stumm, 1987). Site densities are often expressed in terms of sites m^{-2} solid, which is equivalent to $\phi C_S^{tot}/S_{sp}$, where ϕ is porosity (0.347) and S_{sp} is the surface area per unit of bulk volume ($5.58\ m^2\ L^{-1}$). Substitution of values yields $12.4\ \mu mol\ m^{-2}$, which is within the range of 7.5–14.9 $\mu mol\ m^{-2}$ calculated for OH^- site concentration in silica proposed by Hohl et al. (1980) and Schindler and Stumm (1987).

Fe isotope composition vs time profiles for the 208 and 1900 μM experiments at pH 1 and the 208 μM experiment at pH 2 are shown in Fig. 5. The isotopic measurements of the fluid for both series of experiments at pH 1 (Fig. 5a–b) show initially negative values during the sorption phase, with δ^{56}Fe values as low as approximately −1.5‰. As the surface sites become saturated, values increase to around 0‰ (i.e., the input solution δ^{56}Fe value rep-

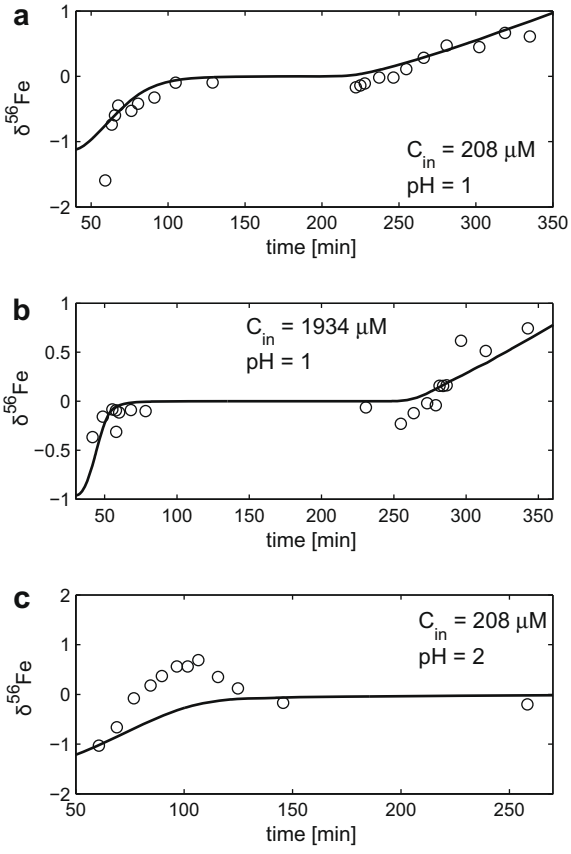

Fig. 5. Evolution of δ^{56}Fe for different experimental conditions. Inlet concentrations (C_{in}) and pH are indicated for each experiment: (a) Fe = 208 μM, pH 1; (b) 1934 μM, pH 1; and (c) 208 μM, pH 2. The solid lines indicate the fit of the isotope transport model to the isotopic data. Note the deviation of the Fe-isotopic compositions from the model calculation as the system reaches the saturation stage predicted by the model.

resenting the equilibrium plateau stage), and during desorption δ^{56}Fe becomes positive, although values do not exceed 1‰. However, in the experiment at 208 μm and pH 2 a different pattern is observed (Fig. 5c): δ^{56}Fe values increase from −1.5‰ to ~1‰ during the sorption phase, although this peak subsides, with values stabilizing at the input solution value of around 0‰ at a later stage, as observed in the other sorption experiments. The positive δ^{56}Fe overstep is most likely a product of irreversible precipitation of Fe-oxhydroxides. Skulan et al (2002) showed that rapid precipitation of Fe(III) oxides from an Fe(III) solution resulted in a negative kinetic iron isotope fractionation ($\Delta^{56}Fe_{Fe\ oxide - Fe(III)aq} = -1.32$ ‰). Such a kinetic fractionation during Fe-oxyhydroxide precipitation would result in heavy isotope enrichment in the solution, as observed in our experiment. Such iron oxide precipitation could irreversibly coat the quartz grains with a film of passive iron oxides. This accounts for the mismatch between the model and Fe concentrations noted earlier for the same experiments (Fig. 4f), and for this reason no isotopic measurements were made of desorption phase (Fig. 5c).

Using the parameters based on the single species sorption model, the isotopic transport model also produces a good fit with the data for different Fe concentrations at pH 1. The kinetic fractionation factor, α_1, is 0.9997 ± 0.0004, while the equilibrium factor, α_e, is 1.0003 ± 0.0001 corresponding to an equilibrium fractionation of $\Delta^{56}Fe_{sorbed\ Fe\text{-}soln} = 0.3$‰ for the Fe sorption-desorption on quartz. The uncertainties are based on an error map (Fig. 6) of over 300 simulations with a range of values for α_e and α_1. The map effectively describes the increase in error relative to the optimum value obtained (i.e., the 50% contour represents an increase of 50% in the difference between the experimental data and the model simulation relative to the lowest value that was obtained), it can be seen that the error function is relatively smooth, converging in the region bounded by the 25% error contour, which serves as a basis for the estimates of the α_1 and α_e uncertainties. The uncertainty for the equilibrium factor is smaller than that for the kinetic factor, reflecting the greater sensitivity of the model to changes in the equilibrium factor. At higher flow rates, producing conditions further from equilibrium, the uncertainty on the kinetic factor should be reduced. The corresponding value of desorption kinetic isotope fractionation factor, α_{-1}, is 0.9994.

Changes in the Fe solution speciation with pH potentially may influence the chemical and isotopic properties of the system. Calculations using equilibrium stability constant data for Fe(III) chloride complexes and the semi-empirical HCl activity model of Bjerrum and Lukes (1986) indicate that speciation will change from dominantly Fe^{3+} at pH 2 to Fe^{3+} ~$FeCl^{2+}$ at pH 1 and $FeCl_2^+ > FeCl^{2+}$ at pH 0. Despite these variations, the experimental Fe concentration data were fit by a single set of sorption kinetic parameters (Table 2), thus implying that the solution

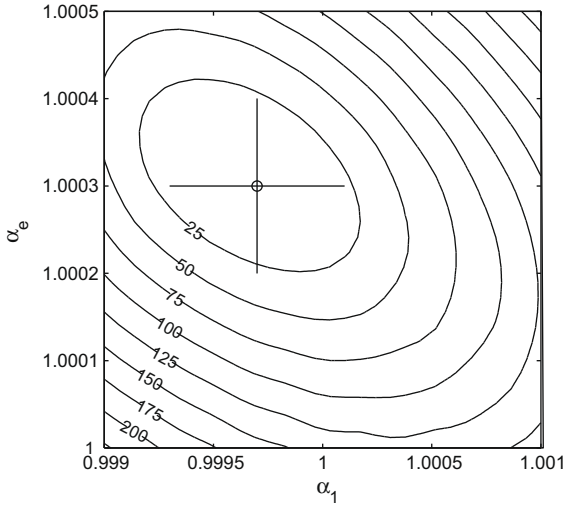

Fig. 6. Error map for different values of α_1 and α_e. The error is given as a percent increase relative to the minimum value (indicated by the circle) at $\alpha_1 = 0.9997$ and $\alpha_e = 1.0003$. Note that the error function is relatively smooth, converging in the region bounded by the 25% error contour, which serves as a basis for the estimated error bars. The contour lines were interpolated from over 300 points using a Delaunay triangulation method.

species changes do not significantly affect the chemical sorption-desorption properties of Fe. Recent theoretical calculations by Hill and Schauble (2008) suggest that the different Fe(III) chloride solution species should isotopically fractionate with respect to one another, with magnitudes up to $\Delta^{56/54}Fe = 2‰$. At HCl strengths of 1.6–3.5 M, experimental studies on Fe-isotope partitioning support the notion of a Fe(III)chloride complex dependent fractionation (Fujii et al., 2006). However, at low chlorinities of 0.1 M or less, experimental studies show no evidence of the fractionation differences predicted by theory (Johnson et al., 2002; Welch et al., 2003), thus suggesting that speciation will not affect isotopic fractionation at these concentrations. Consequently, the values of α_e and α_1 deduced in this study most probably provide good estimates for the equilibrium and kinetic adsorption fractionation factors at pH >1 and low chlorinity.

5. CONCLUSIONS

This study presents a transport model that accounts for the kinetic and equilibrium isotopic fractionations resulting from the sorption–desorption reactions of a tracer metal pulse in a porous medium. The model is successfully applied to a series of experiments in which pulses of NaCl and $FeCl_3$ solutions at different concentrations and pH values 0, 1, and 2 were injected into a water saturated quartz-sand column. By fitting the model to experimental data, the kinetic sorption and desorption Fe concentration parameters and isotope fractionation factors were determined. This has allowed us to explore the relations between the kinetic isotope fractionation and the equilibrium iron isotope fractionation; data not accessible through conventional bulk exchange experiments.

The most pertinent predictions of the model are those pertaining to the Fe-isotopic evolution of the pore fluids in a system evolving through the sequential sorption and desorption processes (Fig. 2). An isotopic depletion marking the initial breakthrough becomes increasingly negative as the value of the kinetic sorption fractionation factor α_1 decreases. In addition, the equilibrium fractionation factor, α_e, determines whether or not $\delta^{56}Fe$ is positive or negative as the system approaches the equilibrium plateau stage, with lower α_e values producing slightly positive $\delta^{56}Fe$ values. During desorption, α_e also controls whether $\delta^{56}Fe$ values are positive or negative at long times; as α_e values increase from unity to 1.001, values of $\delta^{56}Fe$ change from increasingly negative to increasingly positive.

The experimental data are fit by a single set of parameters both for the Fe concentration data as well as the $\delta^{56}Fe$ data (these isotopes representing *ca* 98% of all the iron in the system). The fractionation factors representing a best fit of the transport theory to the Fe concentration data and the $\delta^{56}Fe$ data at pH 1, where Fe^{3+} and $FeCl^{2+}$ are the dominant solution species, are $\alpha_1 = 0.9997 \pm 0.0004$ and $\alpha_e = 1.0003 \pm 0.0001$. The corresponding value of the desorption Fe isotope fractionation factor, α_{-1}, is 0.9994 ($\Delta^{56}Fe_{\text{sorbed Fe}-\text{soln}} = -0.6‰$). Thus, it should be emphasized that both the sorption and desorption processes have fractionation factors <1, and the positive value for the equilibrium fractionation factor arises from the higher value of α_1 relative to α_{-1}. The equilibrium fractionation factor ($\Delta^{56}Fe_{\text{sorbed Fe}-\text{soln}}$) of 0.3‰ is comparable with values deduced for adsorption of metallic cations on iron and manganese oxide surfaces (Balistrieri et al., 2008, Table 2). This implies that sandstone aquifers will fractionate metallic isotope cations through adsorption, as has been predicted for Fe oxides in several studies of natural systems (Teutsch et al., 2005; Busigny and Dauphas, 2007). Moreover, in continental groundwater systems the surface available in sandstone aquifers far outweighs that of Fe-Mn oxides and so adsorption is a potentially major mechanism of metallic isotope fractionation in groundwater metal transport systems. Whether or not the equilibrium fractionation factor is sufficient to describe the system is dependent on the proximity of the system to equilibrium, which is determined by the relative time scales of mass transfer and chemical reaction. Low fluid transport rates should produce a system that is less dependent on kinetic effects.

With the exception of acid mine drainage and some hydrothermal systems, the fractionation factors obtained from our experiments cannot be directly applied to the transport of Fe in groundwater systems because, due to prevalence of higher pH values at which the transport of dissolved Fe only occurs as the reduced ion Fe(II). However, during the Archean highly acidic conditions may have prevailed at Earth's surface due to elevated atmospheric CO_2 concentrations (Lowe and Tice, 2004; Ohmoto et al., 2004), and Fe isotopes in quartz sediments formed at that time could have been strongly influenced by the processes described here. Furthermore, our data may also have implications for Mars where acidic oxidizing ground and surface waters have been proposed (Klinghoffer et al 2004; Grotzinger et al., 2005; McClennan et al., 2005; Squyres and Knoll, 2005; Squyres et al., 2006). Chemical weathering of olivine basalts, erosion and redeposition by such acidic oxidizing waters has given rise to the formation of fine-grained siliclastic and evaporitic sandstones containing minerals such as Mg sulphate (epsomite), gypsum, ferric sulphate (jarosite) and hematite. The occurrence of the jarosite-gypsum assemblage indicates pH conditions of 2–4 (Elwood Madden et al., 2005), and the presence of rare hydrated ferric sulphate minerals rhomboclase and ferricopiapite with epsomite may indicate pH values as low as 0 or less (Tosca et al., 2008). The recent detection of silica-rich deposits in the soils and bedrock at Meridium Planum Home Plate provides further confirmation of chemical element mobilization under acidic sulphate hydrothermal conditions (Squyres et al., 2006 and references cited therein). If these water-borne sedimentary deposits show similar sorption properties to those described here for Fe(III) solutions, sorption may have a role to play in Fe isotope fractionation on Mars in addition, or as an alternative, to the potential role that has been suggested for astrobacterial processes (Chan et al., 2006).

ACKNOWLEDGMENTS

The research was supported by a Grant #2002/338 from the United States Israel Binational Science Foundation. The work of

Simon Emmanuel was generously supported by a Bateman Post-doctoral Fellowship at Yale University. A.M. is Raymond F. Kravis Professor of Geology at the Hebrew University. Dr. Irena Segal of the Geological Survey of Israel is thanked for her help with the plasma mass spectrometry. Dr. Silke Severmann, two anonymous reviewers, and the Associate Editor, Dr. Mark Rehkämper, are thanked for their thoughtful and valuable critical comments.

APPENDIX A. SUPPLEMENTARY DATA

Supplementary data associated with this article can be found, in the online version, at doi:10.1016/j.gca.2008.09.019.

REFERENCES

Balistrieri L. S., Borrok D. M., Wanty R. B. and Ridley W. I. (2008) Fractionation of Cu and Zn isotopes during adsorption onto amorphous Fe(III) oxyhydroxide: experimental mixing of acid rock drainage and ambient river water. *Geochim. Cosmochim. Acta* **72**, 311–328.

Bear J. (1972) *Dynamics of Fluids in Porous Media*. Elsevier.

Barling J. and Anbar A. D. (2004) Molybdenum isotope fractionation during adsorption by manganese oxides. *Earth Planet. Sci. Lett.* **217**, 315–329.

Belshaw N. S., Zhu X-K., Guo Y. and O'Nions R. K. (2000) High precision measurement of iron isotopes by Plasma Source Mass Spectrometry. *Int. J. Mass Spectrom.* **197**, 191–195.

Bjerrum J. and Lukes I. (1986) The iron (III) chloride system. A study of the stability constants and of the distribution of the tetrachloro species between organic solvents and aqueous chloride solutions. *Acta Chem. Scand. A* **40**, 31–40.

Blattner P. and Lassey K. R. (1989) Stable isotope exchange fronts, Damkohler numbers and one-dimensional fluid infiltration. *Chem. Geol.* **78**, 381–392.

Brantley S. L., Liermann L. J., Guynn R . L., Anbar A., Icopini G. A. and Barling J. (2004) Fe-isotopic fractionation during mineral dissolution with and without bacteria. *Geochim. Cosmochim. Acta* **68**, 3189–3204.

Busigny V. and Dauphas N. (2007) Tracing paleofluid circulations using iron isotopes: a study of hematite and goethite concretions from the Navajo Sandstone (Utah, USA). *Earth Planet. Sci. Lett.* **254**, 272–287.

Chan M. A., Johnson C. M., Beard B. L., Bowman J. R. and Parry W. T. (2006) Iron isotopes constrain the pathways and formation mechanisms of terrestrial oxide concretions. A tool for tracing iron isotope cycling on Mars. *Geosphere* **2**, 324–332.

Clayton R. E., Hudson-Edwards K. A. and Houghton S. L. (2005) Isotopic effects during Cu adsorption onto goethite. *Geochim. Cosmochim. Acta* **69**, A216.

Crosby H. A., Johnson C. M., Roden E. E. and Beard B. L. (2005) Coupled Fe(II)–Fe(III) electron/atom exchange as a mechanism for Fe isotope fractionation during dissimilatory iron oxide reduction. *Environ. Sci. Technol.* **39**, 6698–6704.

Crosby H. A., Roden E. E., Johnson C. M. and Beard B. L. (2007) The mechanisms of iron isotope fractionation produced during dissimilatory Fe(III) reductions by *Shewanella putrefaciens* and *Geobacter sulfurreducens*. *Geobiology* **8**, 169–189.

Domenico P. A. and Schwartz F. W. (1997) *Physical and Chemical Hydrogeology*, 2nd ed. John Wiley and Sons Inc.

Ellis A. S., Johnson T. M. and Bullen T. D. (2004) Using chromium stable isotope ratios to quantify Cr(VI) reduction: lack of sorption effects. *Environ. Sci. Technol.* **38**, 3604–3607.

Elwood Madden M. E., Bodnar R. J. and Rimstidt J. E. (2005) Jarosite as an indicator of water-limited chemical weathering on Mars. *Nature* **431**, 821–823.

Fetter C. W. (1988) *Applied Hydrogeology*. Macmillan, NY.

Fujii T., Moynier F., Telouk P. and Albarède F. (2006) Isotope fractionation of Fe(III) in chemical exchange reactions using solvent extraction with crown ether. *J. Phys. Chem. A* **110**, 11108–11112.

Galy A., Pokrovsky O. S. and Schott J. (2002) Ge-isotopic fractionation during its adsorption on goethite: an experimental study. *Geochim. Cosmochim. Acta* **66**, A259.

Grotzinger J. P. et al. (2005) Stratigraphy and sedimentology of a dry to wet eolian deposition system, Burns Formation, Meridiani Planum, Mars. *Earth Planet. Sci. Lett.* **240**, 11–72.

Hill P. S. and Schauble E. (2008) Modeling the effects of bond environment on equilibrium iron isotope fractionation in ferric aquo-chloro complexes. *Geochim. Cosmochim. Acta* **72**, 1939–1958.

Hohl H., Sigg L. and Stumm W. (1980) Characterization of surface chemical properties of oxides in natural waters. In *Particulates in Water* (eds. M. C. Kavanaugh and J. O. Leckie). American Chemical Society, Washington, pp. 1–31.

Icopini G. A., Anbar A. D., Ruebush S. S., Tien M. and Brantley S. M. (2004) Iron isotope fractionation during microbial reduction of iron the importance of adsorption. *Geology* **32**, 205–208.

Johnson C. M., Skulan J. M., Beard B. L., Sun H., Nealson K. H. and Braterman P. S. (2002) Isotopic fractionation between Fe(III) and Fe(II) in aqueous solutions. *Earth Planet. Sci. Lett.* **195**, 141–153.

Johnson C. M., Roden E. E., Welch S. A. and Beard B. L. (2005) Experimental constraints on Fe isotope fractionation during magnetite and Fe carbonate formation coupled to dissimilatory hydrous ferric oxide reduction. *Geochim. Cosmochim. Acta* **69**, 963–993.

Johnson C. M., Beard B. L. and Roden E. E. (2008) The iron isotope fingerprints of redox and biogeochemical cycling in the modern and ancient earth. *Annu. Rev. Earth Planet. Sci.* **36**, 457–493.

Johnson T. M., Herbel M. J., Bullen T. D. and Zawislanski P. T. (1999) Selenium isotope ratios and indicators of selenium sources and oxyanion reduction. *Geochim. Cosmochim. Acta* **63**, 2775–2783.

Juillot F., Maréchal C., Ponthieu M., Cacaly S., Moria G., Benedetti M., Hazemann J. L., Proux O. and Guyot F. (2008) Zinc isotopic fractionation caused by sorption on goethite and 2-Lines ferrihydrite. *Geochim. Cosmochim. Acta* **72**, 4886–4900.

Klinghoffer G. et al. (2004) Jarosite and hematite at Meridiani Planum from opportunity's Mossbauer spectrometer. *Science* **306**, 1740–1745.

Levi L. (2005) Iron transport in saturated porous media: a laboratory study. M.Sc. Thesis, Hebrew University of Jerusalem, 75 p.

Lowe D. R. and Tice M. M. (2004) Evidence for Archean atmospheric and climatic evolution: fluctuating levels of CO_2, CH_4, and O_2 with an overriding tectonic control. *Geology* **32**, 493–496.

Malinovsky D., Hammarlund D., Ilyashuk B., Martinsson O. and Gelting J. (2007) Variations in the isotopic composition of molybdenum in freshwater lake systems. *Chem. Geol.* **236**, 181–198.

Matthews A., Morgans-Bell H., Emmanuel S., Jenkyns H. C., Erel Y. and Halicz L. (2004) Controls of iron isotope fractionation in organic-rich sediments (Kimmeridge Clay, Upper Jurassic, southern England). *Geochim. Cosmochim. Acta* **68**, 3107–3123.

McClennan S. M. et al. (2005) Provenance and diagenesis of outcrops at Meridiani Planum. *Earth Planet. Sci. Lett.* **240**, 95–121.

Ohmoto H., Watanabe Y. and Kumazawa K. (2004) Evidence from massive siderite beds for a CO_2-rich atmosphere before 18 billion years ago. *Nature* **429**, 395–399.

Pokrovsky O. S., Viers J. and Freydier R. (2005) Zn stable isotope fractionation during its adsorption on oxides and hydroxides. *J. Colloid Interface Sci.* **291**, 192–200.

Pokrovsky O. S., Viers J., Emnova E. E., Kompantseva R. and Freydier R. (2008) Copper isotope fractionation during its interaction with soil and aquatic micro-organisms and metal oxy(hydr)oxides: possible structural control. *Geochim. Cosmochim. Acta* **72**, 1742–1757.

Rehkämper M., Frank M., Hein J. R., Porcelli D., Halliday A. N., Ingri J. and Liebtrau V. (2002) Thallium isotope variations in seawater and hydrogenetic, diagenetic, and hydrothermal ferromanganese deposits. *Earth Planet. Sci. Lett.* **197**, 65–81.

Schindler P. W., Fürst B., Dick R. and Wolf P. U. (1976) Ligand properties of surface silanol groups I surface complex formation with Fe^{3+}, Cu^{2+}, Cd^{2+} and Pb^{2+}. *J. Colloid Interface. Sci.* **55**, 469–475.

Schindler P. W. and Stumm W. (1987) The Surface chemistry of oxides, hydroxides and oxide minerals. In *Aquatic Surface Chemistry* (ed. W. Stumm). John Wiley and Sons, pp. 83–107.

Skulan J. L., Beard B. L. and Johnson C. M. (2002) Kinetic and equilibrium Fe isotope fractionation between aqueous Fe(III) and hematite. *Geochim. Cosmochim. Acta* **66**, 2995–3015.

Squyres S. W. and Knoll A. H. (2005) Sedimentary rocks at Meridiani Planum: origin, diagenesis, and implications for life on Mars. *Earth Planet. Sci. Lett.* **240**, 1–10.

Squyres S. W. et al. (2006) Two years at the Meridiani Planum: results from the Opportunity Rover. *Science* **313**, 1403–1407.

Sverjensky D. A. and Sahai N. (1996) Theoretical prediction of single-site surface-protonation equilibrium surface constants for oxides and silicates in water. *Geochim. Cosmochim. Acta* **60**, 3773–3797.

Stumm W. and Morgan J. (1996) *Aquatic Chemistry: Chemical Equilibria and Rates in Natural Waters*. John Wiley and Sons, Inc., NY.

Teutsch N., Von Gunten U., Porcelli D., Cirpka O. A. and Halliday A. N. (2005) Adsorption as a cause for iron isotope fractionation in reduced groundwater. *Geochim. Cosmochim. Acta* **69**, 4175–4185.

Tosca N. J., Knoll A. H. and McLennan S. M. (2008) Water activity and the challenge of life on Early Mars. *Science* **320**, 1204–1207.

Welch S. A., Beard B. L., Johnson C. M. and Braterman P. S. (2003) Kinetic and equilibrium Fe isotopic fractionation between aqueous Fe(II) and Fe(III). *Geochim. Cosmochim. Acta* **67**, 4231–4250.

Zhu X.-K., Guo Y., Williams R. J. P., O'Nions R. K., Matthews A., Belshaw N., Canters G. W., de Waal E. C., Weser U., Burgess B. K. and Salvato B. (2002) Mass fractionation of the transition metal isotopes. *Earth Planet. Sci. Lett.* **200**, 47–62.

Associate editor: Mark Rehkamper